Spatial and temporal expansion of global fire activity in response to climate change

Martín Senande-Rivera (martin.senande.rivera@usc.es)
Universidade de Santiago de Compostela https://orcid.org/0000-0002-2675-3196
Damián Insua-Costa
Universidade de Santiago de Compostela
Gonzalo Miguez-Macho
Universidade de Santiago de Compostela https://orcid.org/0000-0002-4259-7883

Article

Keywords: Global Warming, Wildfire Potential, Fire Season Severity, Boreal, Temperate, Tropical, Arid

Posted Date: March 1st, 2021

DOI: https://doi.org/10.21203/rs.3.rs-143619/v1

Version of Record: A version of this preprint was published at Nature Communications on March 8th, 2022. See the published version at https://doi.org/10.1038/s41467-022-28835-2.

Spatial and temporal expansion of global fire activity in response to climate change

Martín Senande-Rivera[1*], Damián Insua-Costa[1] and Gonzalo Miguez-Macho[1].

[1]Nonlinear Physics Group, Faculty of Physics, Universidade de Santiago de Compostela, Galicia, Spain.

*Correspondence to: martin.senande.rivera@usc.es

Global warming is expected to alter wildfire potential and fire season severity, but the magnitude and location of change is still unclear. Here, we show that climate largely determines present fire-prone regions and their fire season. We categorize these regions according to the climatic characteristics of their fire season into four classes, within general Boreal, Temperate, Tropical and Arid climate zones. Based on climate model projections, we assess the modification of the fire-prone regions in extent and fire season length at the end of the 21st century. We find that due to global warming, the global fire-prone area will increase by 27%, mostly in Boreal (+95%) and Temperate (+17%) zones, where there will also be significant lengthenings of the potential fire season. Our estimates of the global expansion of fire-prone areas highlight the large but uneven impact of a warming climate on Earth's environment.

Wildfires produce important impacts on ecosystems and societies worldwide[1]. Global fire patterns are determined by climate and fuel availability, along with the existence of ignition agents and human factors[2]. At the same time, fires also modify climate through the emission of aerosols and greenhouse gases, and the biosphere by biomass burning[3,4]. As a natural process, fire plays a role in some ecosystems, such as being a regulator of biomass in savanna biomes[5]. It is also used as a management tool in pastoral and agricultural areas with regular

ignitions from humans[6]. Fire can be a hazard to the environment and to human health, especially during extreme fire events, which have substantial economic, social and ecosystemic impacts[7].

There is evidence of a greater influence of climate than of human activities on global biomass burning during the Holocene across multiple spatial and temporal scales[8]. Many studies have focused on quantifying the impact of different climatic and human factors controlling global fire activity[9-12]. The variability in global interannual fire response to climate variables has also been previously analysed[13,14]. The general conclusion emerging from these investigations is that climate related, rather than human factors, are the major controls in global fire activity, and in particular fuel availability (usually quantified by net primary production, NPP) and precipitation[9,12]. Given the strong relationship between fire and climate, climate change resulting from increased greenhouse gas emissions is expected to alter the spatial distribution of fire activity. Some studies point to increases in the severity of the fire season[15] and the wildfire potential[16], and a gradual shift to a global fire regime dominated by temperature[17], rather than precipitation or human factors, at the end of the 21st century. However, the magnitude and location of change is still debated for many parts of the world[18].

This study aims at (1) demonstrating that through simple climate indicators we can reproduce and explain the present global pattern of fire-prone regions and (2) subsequently use the trends in these indicators to infer future potential changes in the extent of fire activity. We focus on the climate-fire relationship, disregarding interannual variability, ignition elements and human factors (when not related to climate, e.g. some agricultural practices). The underlying hypothesis is that there is a high probability of observed fire occurrence wherever a favourable climatic fire setting exists, regardless of the nature of the ignition agent.

Present fire-climate classification

To identify the different regions of the planet with suitable climatic conditions for fire activity, we compare the global distribution of climate indicators based on temperature and precipitation, with satellite-derived GFED4 burned area data[19] (Fig. 1). Starting from four general climates (A-tropical, B-arid, C-temperate and D-boreal) based on the Köppen-Geiger climate classification main categories[20], we create four fire-prone classes using climate thresholds to define the patterns observed in Fig. 1. Each category is characterized by the element that boosts fire activity during the fire season (FS): low precipitation, high temperatures or a combination of both. The classification is made by contrasting the probability distribution of the climatic variables at fire-affected vs. fireless months within each general climate class.

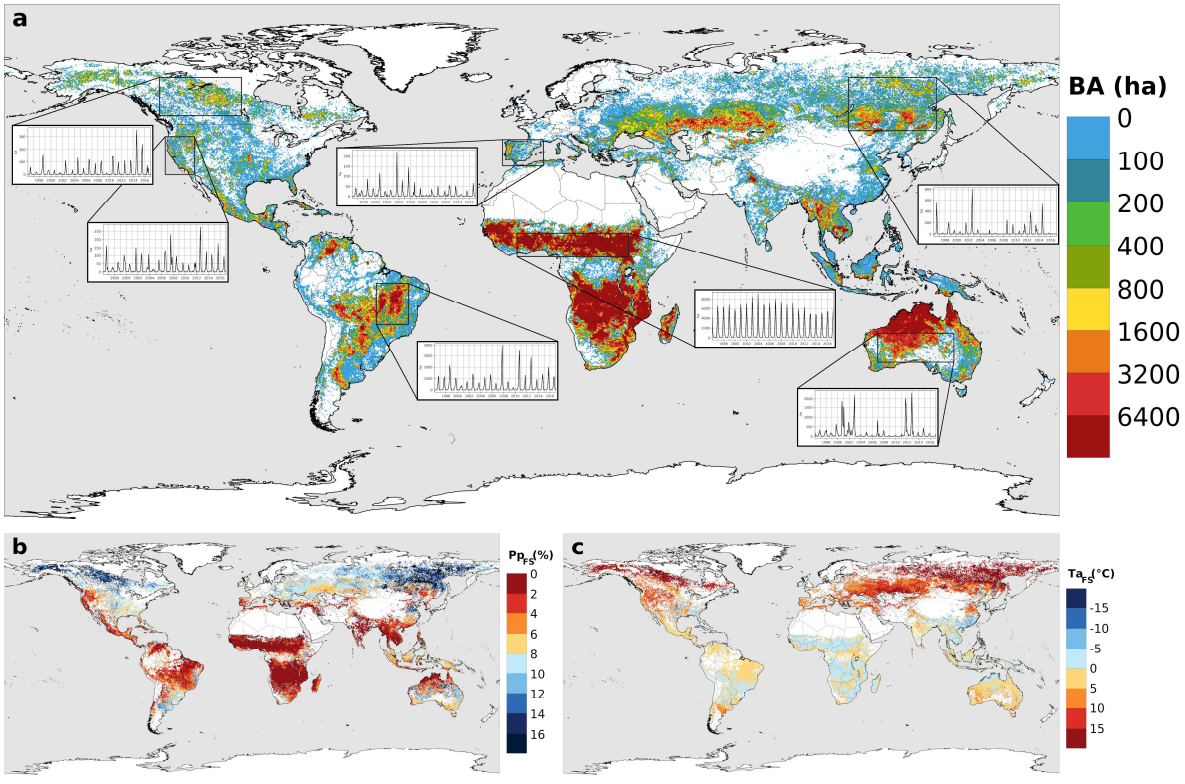

Figure 1. a, **Burned area observations and climate drivers**. Mean annual burned area (BA) and 1996-2016 monthly burned area time series for selected regions. **b**, Average monthly precipitation percentage from the annual total for the fire season (PP_{FS}). **c**, Average monthly temperature anomaly from the annual mean for the fire season (TA_{FS}).

64 The environmental conditions associated with fire occurrence emerge more clearly in this
65 comparison, yielding the different threshold sets in Tab. 1 that determine the fire-prone
66 months at any location (the selection method is detailed in the Supplementary material). We
67 define the number of months classified as fire-prone for each spatial point as the potential fire
68 season length (PFSL), i.e. the season with climatic characteristics prone to fire activity. It is
69 important to distinguish between the FS (fire season, obtained from burned area data) which
70 encompasses the period with most burned area and the PFS (potential fire season, obtained
71 from climatic data), which includes all months when fire conditions exist, regardless of the
72 burned area relative extent.

73 Fig. 2a depicts the global map of burned area classified according to the selected thresholds
74 (Tab. 1). Savanna fires are responsible for the largest proportion of burned area at the global
75 scale[19]. The FS in these areas is longer than in other climates (see Supplementary Fig. S1)
76 and is tied to a pronounced seasonal cycle of precipitation[21-23], with fire occurring mainly
77 during the dry part of the cycle. Because of this, the Tropical - dry season fire class (A-ds)
78 coincides with the distribution of the tropical savanna climate. In Fig. 2, boreal fires are
79 represented as hot season fires (D-hs) due to the large positive temperature anomaly existing
80 in those locations during the FS (Fig. 1c). In fact, temperature variations explain much of the
81 variability in boreal burned area[24,25]. Temperate fires are classified as dry and hot season (C-
82 dhs) because they affect regions where the dry season coincides with the warm season (Fig
83 1b, 1c). Here, high temperatures and precipitation seasonality determine fire activity and
84 inter-annual burned area variability, e.g. in Western North America[26-29] and Southern
85 Europe[30,31]. Fire activity in arid regions occurs during warm months, but the relation with
86 precipitation is more complex. The fire season is associated with a hot season in cooler
87 (MAT<18°C) midlatitude arid areas where no clear wet period is observed, e.g. the Western
88 US and Central Asia (Supplementary Fig. S5 and S6), but closer to the tropics where it is

89 warm year-round, it can be also determined by the existence of a marked annual wet and dry
90 season cycle, with fires occurring sometime during the dry season. In the warmest arid
91 regions (MAT>27°C), the fire season starts right at the beginning of the dry season (e.g. the
92 Sahel, Supplementary Fig. S8) while where MATs are more moderate, between 18°C and
93 27°C, it takes longer to develop (e.g. Central Australia and the Kalahari desert,
94 Supplementary Fig. S7 and S8). Due to the dependency between fires and the timing of
95 precipitation and temperatures in arid climates, we named this class as Arid dry and hot
96 season (B-dhs). A more in-depth discussion about the definition of this fire-climate class can
97 be found in the Supplementary material.

98 In Fig. 2b we classify every spatial point and not only those with burned area observations as
99 in Fig. 2a. The four groups in Fig 2a show observed fire locations that share some specific
100 climate conditions, and the classification in Fig. 2b shows the world areas were these
101 conditions occur for at least one month. The great match between these two maps reveals a
102 two-way relation between fires and climate: fires take place under specific climatic
103 conditions, and most places with these climatic conditions are indeed fire prone, which
104 confirms our earlier hypothesis. Fire activity is controlled by weather, resources to burn and
105 ignitions, as represented through the fire regime triangle[11,18]. On broad temporal scales and
106 large spatial scales, temperature and precipitation have an important impact on fire because
107 these climate variables influence vegetation type and the abundance, composition, moisture
108 content, and structure of fuels[32]. Furthermore, ignitions do not seem to limit fire activity at
109 coarse spatial and temporal resolutions, implying that, where fuels are sufficient and
110 atmospheric conditions are conducive to combustion, the potential for ignition exists, either
111 by lightning or human causes[12,18]. For all these reasons, we can identify specific climates that
112 are prone to fires.

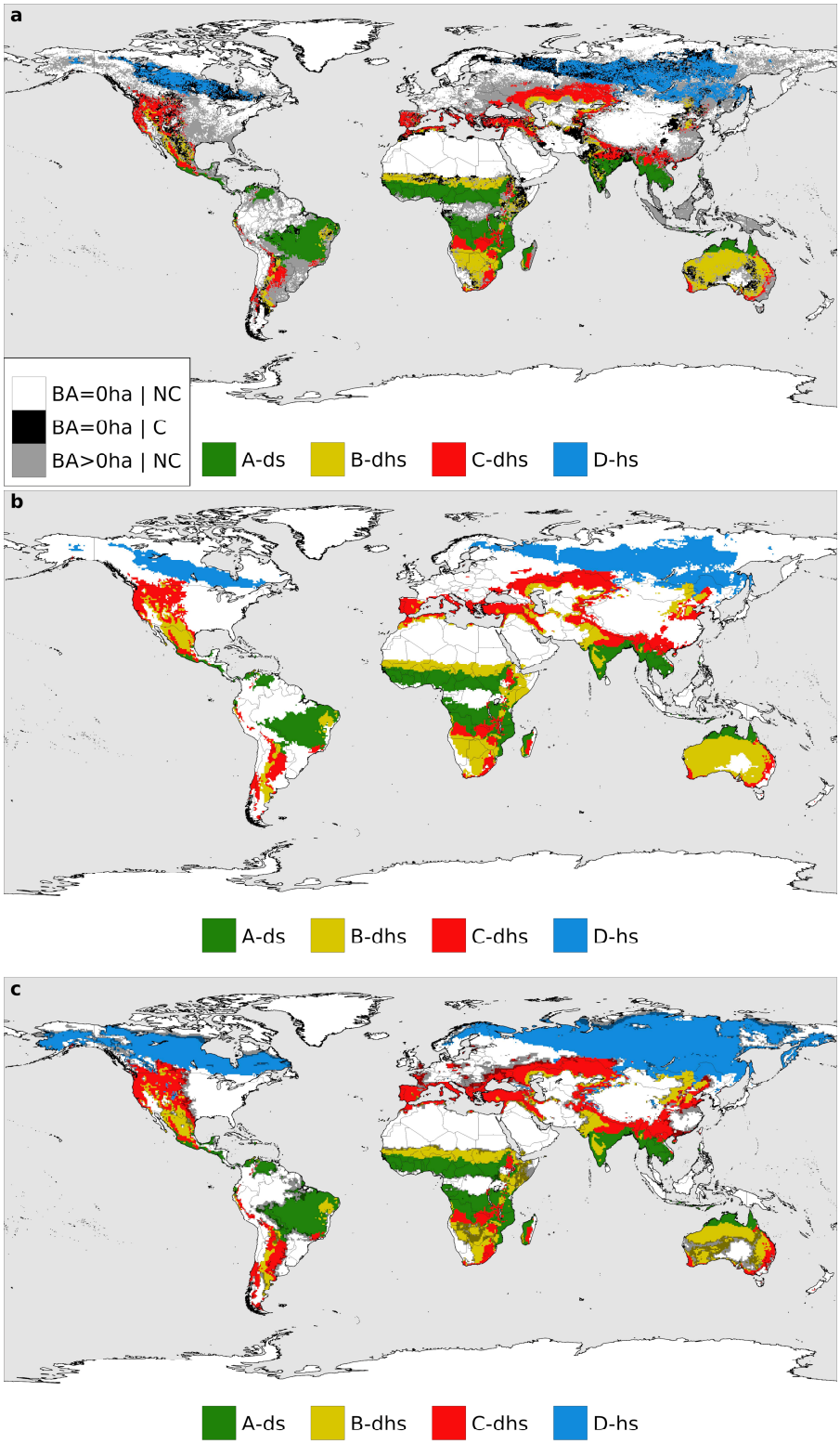

Figure 2. Fire-prone region classification. a, With observed burned area (BA) data as a reference: Not classified (NC, white) and misclassified (C, black) areas with BA=0ha, unclassified (NC, grey) and classified (A-ds, B-dhs, C-dhs and D-hs) areas with BA>0ha. **b**, Present (1996-2016) fire-prone climatic regions. **c**, Future (2070-2099) fire-prone climatic regions with shaded grey representing a <75% confidence percentage, estimated as the percentage of CMIP5 Global Circulation Models (GCMs) agreeing on the result.

The areas classified as fire-prone in Fig. 2b comprise 94.7% of the observed global mean annual burned area in Fig. 1. Furthermore, the PFS obtained in the fire-climate classification (Fig. 3b) also correlates well with the timing of observed fire incidence, as globally 84.2 % of the observed mean burned area occurs during the identified months of PFS at classified fire-prone locations. Unclassified regions (in grey in Fig. 2a) correspond for the most part to those with the least burned area, those where agricultural practices modify the climatic seasonality of fires, or those where fires, though may be severe, occur sporadically and not every year. A detailed discussion about the reliability of the method is included in the Supplementary material.

Future fire-climate classification

A future fire-climate classification map is derived by applying the thresholds obtained in the present fire-climate classification to future climatology variables from multiple Coupled Model Intercomparison Project Phase 5 (CMIP5) Global Circulation Model (GCM) outputs, considering the RCP8.5 scenario. Two contrasting approaches can be taken for analysing future fire activity, one that considers quick vegetation adaptation to the new climatic conditions, and another that does not. These two approaches clearly diverge in the boreal regions, where the biome (mainly taiga) is strongly conditioned by the low temperatures and where future temperature changes at the end of the 21st century will have a greater amplitude. It is expected that the boreal forest of these areas will not be immediately replaced by a temperate mixed forest where the average annual temperature exceeds the range of values typical of the taiga biome. Terrestrial vegetation compositional and structural change could occur during the 21st century where vegetation disturbance is accelerated or amplified by human activity, but equilibrium states may not be reached until the 22nd century or beyond[33].

Based on the assumption that during the future period (2070-2099) the vegetation will not be fully adapted to the new climatic conditions, and since the present Köppen-Geiger climate classification (on which we base our A, B, C and D categories) closely corresponds to the different existent biomes[20], we analyse only the projected changes in the specific fire-climate classification variables, maintaining the general division of Tropical, Arid, Temperate and Boreal regions as is in present climate conditions. The future fire-climate classification is shown in Fig. 2c.

Future changes in global fire activity

Modelled future fire-prone regions experience significant variations with respect to the present (Fig. 2b, 2c). Due to global warming, the D-hs fire class pertaining to boreal forests will spread over a larger area, reaching most of Northern Scandinavia and undergoing a southward and northward expansion in Canada, Alaska and Russia. This category will experience a percentual expansion of 94.9% according to our results.

The C-dhs fire class of midlatitudes also undergoes a considerable expansion of 17.1% in area (Fig. 2b, 2c). The most remarkable changes are expected in Southern China, Eastern Australia, Southern Africa and Southern Europe. In addition, a large part of Europe presents low confidence in some non-fire prone regions, indicating that some models predict for them an evolution from a non-fire to a fire-prone category with Csa and Csb Mediterranean climates[34].

The A-ds fire class in the Tropics presents the least spatial changes (Fig. 2b, 2c), with an expansion of 4.5%. The most important differences are found in South America. Some of the climate model results considered here indicate also that some parts of the Eastern Amazon rainforest will move from a non-fire class to A-ds fire class, as other studies have suggested[35].

The Arid fire-prone class (B-dhs) will reduce its area by 8.7%. This contraction is mainly caused by the decrease in MAP values in Central Australia, conducive to desertification and vegetation, hence fuel, reduction. However, there is significant uncertainty in this region (Fig. 2c).

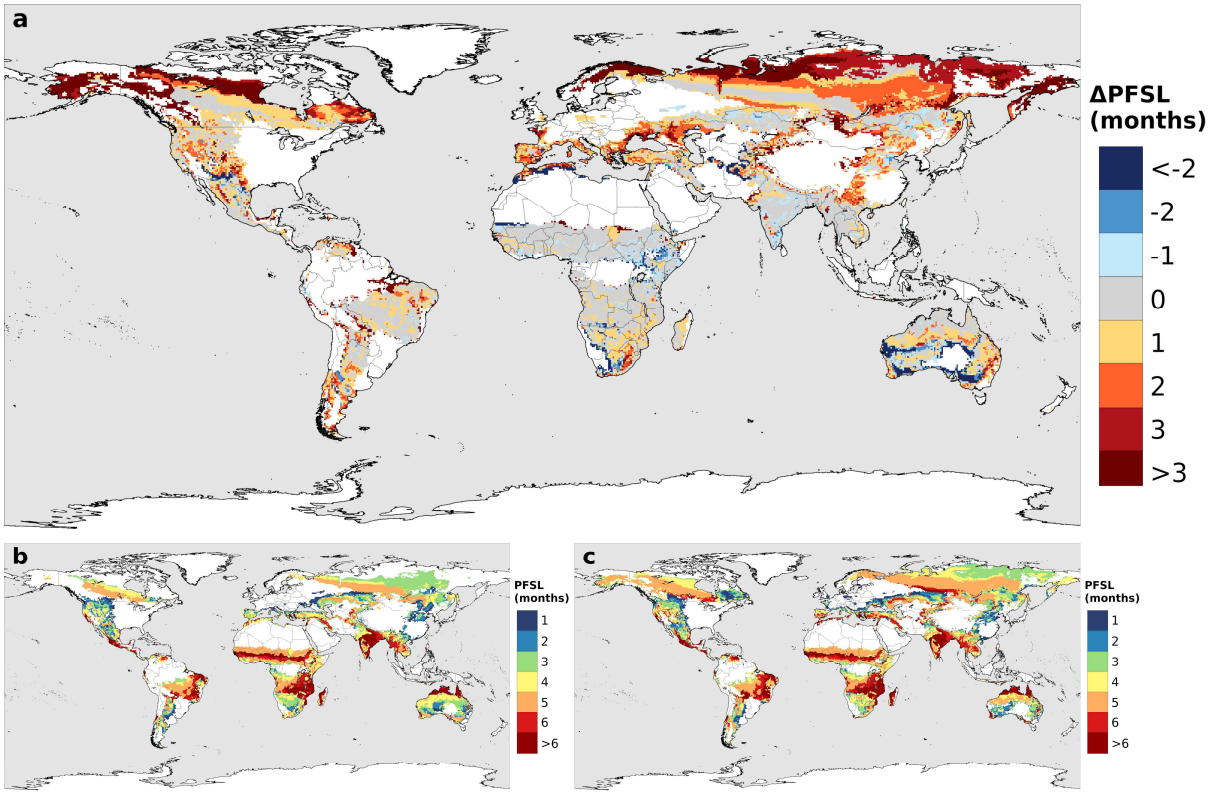

Figure 3. Potential Fire Season. a Future minus present Potential Fire Season Length (PFSL) difference in months (ΔPFSL). **b**, Present Potential Fire Season. c, Future Potential Fire Season.

Clearer conclusions can be drawn from the PFSL calculation (Fig. 3). The number of months meeting the set of conditions in Tab. 1 yields the estimated PFSL (Fig.3b). In the boreal regions, we obtain a general lengthening of the PFS. The PFS of these areas is conditioned by temperature, so the amplified warming of Artic zones[36] is expected to make the FS longer. Notwithstanding, in certain parts of Eastern Asia, the intense warming is counterbalanced by an increase of the precipitation in certain warm months (see Supplementary Fig. S18, S19), leading to a slight shortening of our estimated PFS. There is evidence, however, that

183 temperature increases may lead to drier fuels in the future despite the precipitation increase,
184 thus augmenting fire-risk, as some investigations have shown for Canada[37]. Our results agree
185 in general with several other studies that have previously pointed towards an increase of the
186 FSL in boreal areas[2,15,38], even when some suggest a more pronounced lengthening in more
187 northerly latitudes[2,15].

188 The C-dhs fire class, corresponding to temperate climates, will also experience a general
189 lengthening of the PFS (Fig. 3). A future precipitation decline will be especially significant in
190 Southern Europe (Supplementary Fig. S16), associated with an increased anticyclonic
191 circulation yielding more stable conditions[39], while the temperature raise will be quite
192 homogeneous among all C-dhs fire-climate class areas. The FS drought intensification around
193 the Mediterranean, together with the general warming (Supplementary Fig. S17), will lead to
194 a lengthening of the PFS of around 2 months (Fig. 3a), but present PFS months will also
195 experience this precipitation decline (Supplementary Fig. S19), meaning that the FS will be
196 more severe. The Western US, which has already experienced over the last decades the
197 lengthening of the FS[40] and the increase of large fires[41] and extreme wildfire weather[42] due to
198 climate change, will also experience a FS lengthening by the end of the 21st century. Some
199 authors[16,43,44] have studied projected fire future changes from other points of view
200 (occurrence of very large fires, wildfire potential, etc.), finding also a general increase of fire
201 severity by the end of the century in some of these C-dhs fire regions.

202 The PFSL of the Tropical A-ds fire-climate class presents slight differences between present
203 and future values (Fig. 3). Some areas of the Eastern African savanna will experience a
204 shortening of the PFS, while Southern Africa shows a lengthening. A dipole pattern of
205 wetting in tropical Eastern Africa and drying in Southern Africa[45] could be the reason of
206 these future changes. There is a contrasted influence of ENSO in present African fire
207 patterns[46], which suggests that the future pattern of precipitation variations in Central Africa

maybe associated with ENSO future changes under climate change conditions[47]. Although the quantification of ENSO changes in a warmer climate is still an issue that continues to be investigated, an expansion and strengthening of ENSO teleconnections is confirmed by some authors[48,49].

Our results show that fire-prone areas in Temperate and especially Boreal climates, are projected to undergo the most significant expansion and lengthening of the potential fire season at the end of the XXI century driven by rising temperatures. In the Tropics, little change is expected in these respects. Notwithstanding, global warming is likely to make fire risk more severe mostly everywhere, and in particular in some regions such as Mediterranean Europe and the Eastern Amazon, where an important decrease in precipitation is also predicted during the PFS (Fig. S19). More favourable fire conditions will potentially increment fire activity and burned area in many places. In others, especially in the Tropics, increasing suppression efforts and a cease to agricultural and pastoral practices like vegetation clearing by fire, replaced by more intensive farming, could counteract the impact of a warmer climate. A reduction of these human caused fires in the Tropics could bring global burned area down[1], despite rising trends elsewhere, given the disproportionate share of Tropical fires in burned area at the global scale (Fig.1).

References

1. Andela, N. *et al.* A human-driven decline in global burned area. *Science* **356**, 1356-1362 (2017).
2. Flannigan, M. D., Krawchuk, M. A., de Groot, W. J., Wotton, B. M. & Gowman, L. M. Implications of changing climate for global wildland fire. *Int. J. Wildland Fire* **18**, 483-507 (2009).
3. Bowman, D. M. *et al.* Fire in the Earth system. *Science* **324**, 481-484 (2009).

4. Langmann, B., Duncan, B., Textor, C., Trentmann, J. & Van der Werf, G. R. Vegetation fire emissions and their impact on air pollution and climate. *Atmos. Environ.* **43**, 107-116 (2009).

5. Scholes, R. J. & Archer, S. R. Tree-grass interactions in savannas. *Annu. Rev. Ecol. Syst.* **28**, 517-544 (1997).

6. Cochrane, M. A. Fire science for rainforests. *Nature* **421**, 913-919 (2003).

7. Bowman, D. M. *et al.* Human exposure and sensitivity to globally extreme wildfire events. *Nat. Ecol. Evol.* **1**, 1-6 (2017).

8. Marlon, J. R. *et al.* Global biomass burning: a synthesis and review of Holocene paleofire records and their controls. *Quat. Sci. Rev.* **65**, 5-25 (2013).

9. Aldersley, A., Murray, S. J. & Cornell, S. E. Global and regional analysis of climate and human drivers of wildfire. *Sci. Total Environ.* **409**, 3472-3481 (2011).

10. Jolly, W. M. *et al.* Climate-induced variations in global wildfire danger from 1979 to 2013. *Nat. Commun.* **6**, 1-11 (2015).

11. Krawchuk, M. A. & Moritz, M. A. Constraints on global fire activity vary across a resource gradient. *Ecology* **92**, 121-132 (2011).

12. Krawchuk, M. A., Moritz, M. A., Parisien, M. A., Van Dorn, J. & Hayhoe, K. Global pyrogeography: the current and future distribution of wildfire. *PloS ONE, 4*(4) (2009).

13. Abatzoglou, J. T., Williams, A. P., Boschetti, L., Zubkova, M. & Kolden, C. A. Global patterns of interannual climate–fire relationships. *Glob. Chang. Biol.* **24**, 5164-5175 (2018).

14. Van Der Werf, G. R., Randerson, J. T., Giglio, L., Gobron, N. & Dolman, A. J. Climate controls on the variability of fires in the tropics and subtropics. *Global Biogeochem. Cycles* **22**, GB3028 (2008).

15. Flannigan, M. *et al.* Global wildland fire season severity in the 21st century. *For. Ecol. Manag.* **294**, 54-61 (2013).
16. Liu, Y., Stanturf, J. & Goodrick, S. Trends in global wildfire potential in a changing climate. *For. Ecol. Manag.* **259**, 685-697 (2010).
17. Pechony, O. & Shindell, D. T. Driving forces of global wildfires over the past millennium and the forthcoming century. *Proc. Natl Acad. Sci. USA* **107**, 19167-19170 (2010).
18. Moritz, M. A. *et al.* Climate change and disruptions to global fire activity. *Ecosphere* **3**, 1-22 (2012).
19. Giglio, L., Randerson, J. T. & Van der Werf, G. R. Analysis of daily, monthly, and annual burned area using the fourth-generation global fire emissions database (GFED4). *J. Geophys. Res. Biogeosc.* **118**, 317-328 (2013).
20. Köppen, W. *Das geographische System der Klimate,* 1-44 (Gebrüder Borntraeger: Berlin, Germany, 1936).
21. Cahoon, D. R., Stocks, B. J., Levine, J. S., Cofer, W. R. & O'Neill, K. P. Seasonal distribution of African savanna fires. *Nature* **359**, 812-815 (1992).
22. Archibald, S., Roy, D. P., van Wilgen, B. W., & Scholes, R. J. What limits fire? An examination of drivers of burnt area in Southern Africa. *Glob. Change Biol.* **15**, 613-630 (2009).
23. Van Der Werf, G. R., Randerson, J. T., Collatz, G. J., & Giglio, L. Carbon emissions from fires in tropical and subtropical ecosystems. *Glob. Change Biol.* **9**, 547-562 (2003).
24. Gillett, N. P., Weaver, A. J., Zwiers, F. W. & Flannigan, M. D. Detecting the effect of climate change on Canadian forest fires. *Geophys. Res. Lett.* **31**, L18211 (2004).

25. Flannigan, M. D., Logan, K. A., Amiro, B. D., Skinner, W. R., & Stocks, B. J. Future area burned in Canada. *Clim. Change* **72**, 1-16 (2005).

26. Littell, J. S., McKenzie, D., Peterson, D. L. & Westerling, A. L. Climate and wildfire area burned in western US ecoprovinces, 1916-2003. *Ecol. Appl.* **19**, 1003-1021 (2009).

27. Marlon, J. R. *et al.* Long-term perspective on wildfires in the western USA. *Proc. Natl Acad. Sci. USA* **109**, E535-E543 (2012).

28. Parisien, M. A., & Moritz, M. A. Environmental controls on the distribution of wildfire at multiple spatial scales. *Ecol. Monogr.* **79**, 127-154 (2009).

29. Seager, R. *et al.* Climatology, variability, and trends in the US vapor pressure deficit, an important fire-related meteorological quantity. *J. Appl. Meteor. Climatol.* **54**, 1121-1141 (2015).

30. Sousa, P. M., Trigo, R. M., Pereira, M. G., Bedia, J., & Gutiérrez, J. M. Different approaches to model future burnt area in the Iberian Peninsula. *Agric. For. Meteorol.* **202**, 11-25 (2015).

31. Turco, M. *et al.* On the key role of droughts in the dynamics of summer fires in Mediterranean Europe. *Sci. Rep.* **7**, 1-10 (2017).

32. Hantson, S. *et al*. The status and challenge of global fire modelling. *Biogeosciences*, **13**, 3359-3375 (2016).

33. Nolan, C. *et al.* Past and future global transformation of terrestrial ecosystems under climate change. *Science* **361**, 920-923 (2018).

34. Beck, H. E. *et al.* Present and future Köppen-Geiger climate classification maps at 1-km resolution. *Sci. Data* **5**, 180214 (2018).

35. Bedia, J. *et al.* Global patterns in the sensitivity of burned area to fire-weather: Implications for climate change. *Agric. For. Meteorol.* **214**, 369-379 (2015).

304 36. Pithan, F. & Mauritsen, T. Arctic amplification dominated by temperature feedbacks in
305 contemporary climate models. *Nat. Geosci.* **7**, 181-184 (2014).
306 37. Flannigan, M. D. *et al.* Fuel moisture sensitivity to temperature and precipitation:
307 climate change implications. *Clim. Change* **134**, 59-71 (2016).
308 38. De Groot, W. J., Flannigan, M. D., & Cantin, A. S. Climate change impacts on future
309 boreal fire regimes. *For. Ecol. Manag.* **294**, 35-44 (2013).
310 39. Giorgi, F. & Lionello, P. Climate change projections for the Mediterranean region.
311 *Glob. Planet. Change* **63**, 90-104 (2008).
312 40. Abatzoglou, J. T., & Williams, A. P. Impact of anthropogenic climate change on
313 wildfire across western US forests. *Proc. Natl Acad. Sci. USA* **113**, 11770-11775
314 (2016).
315 41. Dennison, P. E., Brewer, S. C., Arnold, J. D., & Moritz, M. A. Large wildfire trends in
316 the western United States, 1984–2011. *Geophys. Res. Lett.* **41**, 2928-2933 (2014).
317 42. Goss, M. *et al.* Climate change is increasing the likelihood of extreme autumn wildfire
318 conditions across California. *Environ. Res. Lett.* **15**, 094016 (2020).
319 43. Barbero, R., Abatzoglou, J. T., Larkin, N. K., Kolden, C. A. & Stocks, B. Climate
320 change presents increased potential for very large fires in the contiguous United States.
321 *Int. J. Wildland Fire* **24**, 892-899 (2015).
322 44. Turco, M. *et al.* Exacerbated fires in Mediterranean Europe due to anthropogenic
323 warming projected with non-stationary climate-fire models. *Nature commun.* **9**, 1-9
324 (2018).
325 45. Serdeczny, O. *et al.* Climate change impacts in Sub-Saharan Africa: from physical
326 changes to their social repercussions. *Reg. Environ. Change* **17**, 1585-1600 (2017).
327 46. Andela, N. & Van Der Werf, G. R. Recent trends in African fires driven by cropland
328 expansion and El Nino to La Nina transition. *Nat. Clim. Change* **4**, 791-795 (2014).

329 47. Dore, M. H. Climate change and changes in global precipitation patterns: what do we
330 know?. *Environ. Int.* **31**, 1167-1181 (2005).
331 48. Fasullo, J. T., Otto-Bliesner, B. L. & Stevenson, S. ENSO's changing influence on
332 temperature, precipitation, and wildfire in a warming climate. *Geophys. Res. Lett.* **45**,
333 9216-9225 (2018).
334 49. Perry, S. J., McGregor, S., Gupta, A. S. & England, M. H. Future changes to El Niño–
335 Southern Oscillation temperature and precipitation teleconnections. *Geophys. Res. Lett.*
336 **44**, 10608-10616 (2017).

337 **Tables**

338 **Table 1. Fire classification defining criteria.** Fire-climate classes (A-ds, B-dhs, C-dhs and
339 D-hs) must meet general Köppen-Geiger climate criteria (A, B, C and D) and the specific
340 fire-climate thresholds. All variables are defined in Table 2.

A		$MAP \geq 10 \cdot P_{threshold}$ & $Tmin \geq 18°C$
	A - ds	$MAP \geq 225mm$ & $Pmin \leq 20mm$ & $Pm \leq 85mm$
B		$MAP < 10 \cdot P_{threshold}$
	B - dhs	$MAP \geq 225mm$ & $Tm \geq 19°C$ & $Pm \leq 85mm$ if $MAT < 18°C$, all months analysed if $18°C \leq MAT < 27°C$, months with $2 \leq dm_{Pmax} \leq 6$ anlysed if $MAT \geq 27°C$, months with $7 \leq dm_{Pmax} \leq 11$ anlysed
C		$MAP \geq 10 \cdot P_{threshold}$ & $Tmin < 18°C$ & $MAT \geq 2°C$
	C - dhs	$MAP \geq 225mm$ & $Pm \leq 40mm$ & $Tm \geq 12°C$
D		$MAP \geq 10 \cdot P_{threshold}$ & $MAT < 2°C$
	D - hs	$MAP \geq 225mm$ & $Tmax > 15°C$ & $Tm \geq 7°C$ & $Pm \leq 110mm$

341

Table 2. Variable definitions.

Variable	Units	Definition
MAT	°C	Mean annual 2m air temperature
Tmin	°C	Mean 2m air temperature of the coldest month
Tmax	°C	Mean 2m air temperature of the hottest month
Tm	°C	Mean monthly 2m air temperature
MAP	mm	Mean annual precipitation
Pmin	mm	Mean precipitation of the driest month
Pm	mm	Mean monthly precipitation
$P_{threshold}$	mm	$2\times MAT$ if $P_{winter}>70\%$ $2\times MAT+28$ if $P_{summer}>70\%$ $2\times MAT+14$ otherwise
P_{winter}	%	Percentage of MAP that falls during the colder six-month period between April-September and October-March[34]

Methods

Burned area data. To study how climate influences fires at the global scale we use the Global Fire Emissions Database (GFED)[50]. The fourth generation of the GFED burned area data set (GFED4) provides global monthly burned area at the 0.25° spatial resolution from mid-1995 to 2016[19]. This dataset is obtained from the Collection 5.1 MODIS direct broadcast (DB) burned area product (MCD64A1), now generated globally using the MODIS DB burned-area mapping algorithm[51].

Climate data. Climate datasets are acquired from WFDE5[52], WATCH Forcing Data methodology applied to ERA5[53], the fifth generation ECMWF reanalysis for the global climate. This is a meteorological forcing dataset for land surface and hydrological models. The dataset was derived applying sequential elevation and monthly bias correction methods[54]

355 to 0.5° aggregated ERA5 reanalysis products[55]. The monthly observational datasets used for
356 bias correction are the Climate Research Unit gridded station observations CRU TS4.03[56] and
357 the Global Precipitation Climatology Centre gridded station precipitation observations
358 GPCCv2018[57] for rainfall and snowfall rates. From this climate dataset we calculated the
359 annual and monthly temperature and total precipitation (rainfall and snowfall) climatology
360 for the same 1996-2016 period. We downscale these variables to a 0.25° grid using a bilinear
361 interpolation.

362 **GCM data.** For analysing future variations in fire activity, we use the Coupled Model
363 Intercomparison Project Phase 5 CMIP5[58] historical and future projections from 22 climate
364 models. The GCMs are ACCESS1-0, ACCESS1-3, bcc-csm1-1, bcc-csm1-1-m, BNU-ESM,
365 CMCC-CMS, CNRM-CM5, GFDL-CM3, GFDL-ESM2G, GFDL-ESM2M, GISS-E2-H,
366 GISS-E2-H-CC, GISS-E2-R, GISS-E2-R-CC, HadGEM2-CC, inmcm4, IPSL-CM5A-LR,
367 IPSL-CM5A-MR, IPSL-CM5B-LR, MPI-ESM-LR, MPI-ESM-MR and NorESM1-M. We
368 use the RCP8.5[59] greenhouse gas concentration model outputs for the future period. The
369 Representative Concentration Pathway RCP8.5 assumes a scenario in which greenhouse gas
370 emissions continue to increase throughout the 21st century, that lead to a radiative forcing of
371 8.5 Wm^{-2} by 2100[60]. For each model, we only consider the main ensemble member (r1i1p1).
372 We analyze two periods, present (1996-2016) and future (2070-2099). The present period is
373 obtained by concatenating precipitation and temperature historical data (1996-2006) and
374 projected data until 2016 (2006-2016). Future climatology values are obtained with the
375 anomaly method[61]: for each one of the 22 CMIP5 global models, we calculate temperature
376 anomalies and precipitation ratios between 1996–2016 and 2070–2099 and interpolate them
377 from their native model resolution to 0.25° using bilinear interpolation. Finally, future values
378 of the variables of interest were derived from present values by adding the temperature

anomalies to present temperatures and by multiplying the present precipitation by the precipitation ratios.

Threshold selection. The detailed description of the method used to define the thresholds in Table 1 is included in the Supplementary Material.

Data availability. The datasets generated during the current study are available from the corresponding author on reasonable request.

Code availability. The codes used to classify the data according to the criteria in Table 1 are available upon request from the corresponding author.

Methods references

50. Van Der Werf *et al*. Global fire emissions estimates during 1997-2016. *Earth Syst. Sci. Data* **9**, 697-720 (2017).
51. Giglio, L., Loboda, T., Roy, D. P., Quayle, B. & Justice, C. O. An active-fire based burned area mapping algorithm for the MODIS sensor. *Remote Sens. Environ.* **113**, 408-420 (2009).
52. Copernicus Climate Change Service (C3S). Near surface meteorological variables from 1979 to 2018 derived from bias-corrected reanalysis. Copernicus Climate Change Service Climate Data Store (CDS). https://doi.org/10.24381/cds.20d54e34 (2020).
53. Copernicus Climate Change Service (C3S). ERA5: Fifth generation of ECMWF atmospheric reanalyses of the global climate. Copernicus Climate Change Service Climate Data Store (CDS). (2017).
54. Weedon, G. P. *et al.* Creation of the WATCH forcing data and its use to assess global and regional reference crop evaporation over land during the twentieth century. *J. Hydrometeorol.* **12**, 823-848 (2011).

55. Cucchi, M. *et al.* WFDE5: bias adjusted ERA5 reanalysis data for impact studies. *Earth Syst. Sci. Data* **12**, 2097–2120 (2020).

56. Harris, I. P. D. J., Jones, P. D., Osborn, T. J. & Lister, D. H. Updated high-resolution grids of monthly climatic observations–the CRU TS3. 10 Dataset. *Int. J. Climatol.* **34**, 623-642 (2014).

57. Schneider, U., Becker, A., Finger, P., Meyer-Christoffer, A. & Ziese, M. GPCC Full Data Monthly Product Version 2018 at 0.5°: Monthly Land-Surface Precipitation from Rain-Gauges built on GTS-based and Historical Data. Global Precipitation Climatology Centre. (2018).

58. Taylor, K. E., Stouffer, R. J. & Meehl, G. A. An overview of CMIP5 and the experiment design. *Bull. Amer. Met. Soc.* **93**, 485-498 (2012).

59. Riahi, K. et al. RCP 8.5—A scenario of comparatively high greenhouse gas emissions. *Clim. change* **109**, 33-57 (2011).

60. Van Vuuren, D. P. et al. The representative concentration pathways: an overview. *Clim. change* **109**, 5-31 (2011).

61. Teutschbein, C. & Seibert, J. Bias correction of regional climate model simulations for hydrological climate-change impact studies: Review and evaluation of different methods. *J. Hydrol.* **456**, 12-29 (2012).

Acknowledgements

Funding comes from the Spanish Ministerio de Economia y Competitividad OPERMO (CGL2017-89859-R) and the CRETUS strategic partnership (AGRUP2015/02). All these programs are co-funded by the European Union ERDF. M. S. R. acknowledges Xunta de Galicia for a predoctoral grant (Programa de axudas á etapa predoutoral 2019, ED481A-2019/112). D. I. C. was awarded a pre-doctoral FPI (PRE2018-084425) grant from the

Spanish Ministry of Science, Innovation and Universities. Computation took place at CESGA (Centro de Supercomputacion de Galicia), Santiago de Compostela, Galicia, Spain.

Author contributions

M. S. R. designed the study and drafted the manuscript. D. I. C. and G. M. M. provided critical feedback and contributed to writing the paper.

Competing interests

The authors declare no competing interests.

Supplementary information

Supplementary information is available for this paper.

Figures

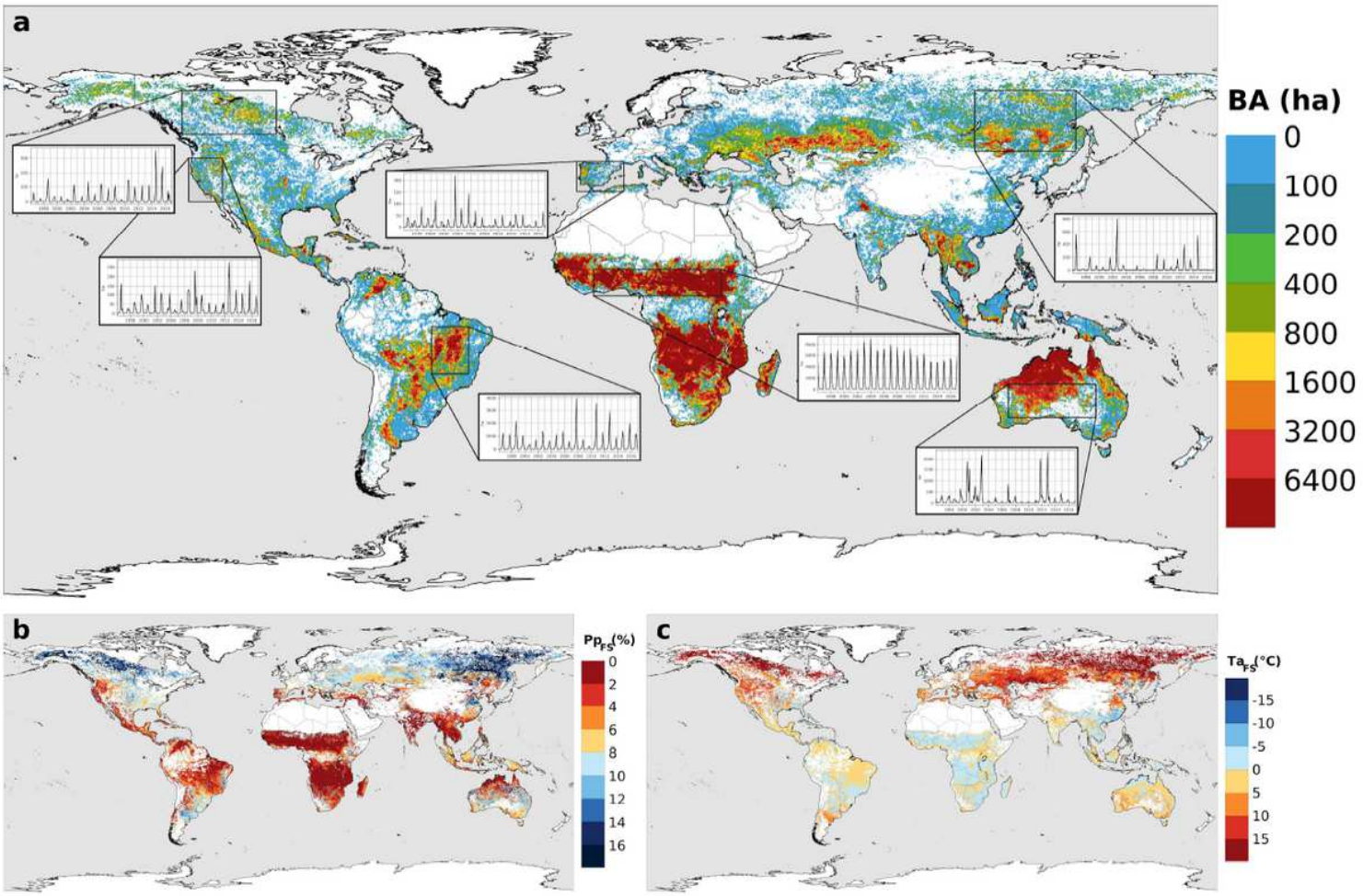

Figure 1

a, Burned area observations and climate drivers. Mean annual burned area (BA) and 1996-2016 monthly burned area time series for selected regions. b, Average monthly precipitation percentage from the annual total for the fire season (PPFS). c, Average monthly temperature anomaly from the annual mean for the fire season (TAFS). Note: The designations employed and the presentation of the material on this map do not imply the expression of any opinion whatsoever on the part of Research Square concerning the legal status of any country, territory, city or area or of its authorities, or concerning the delimitation of its frontiers or boundaries. This map has been provided by the authors.

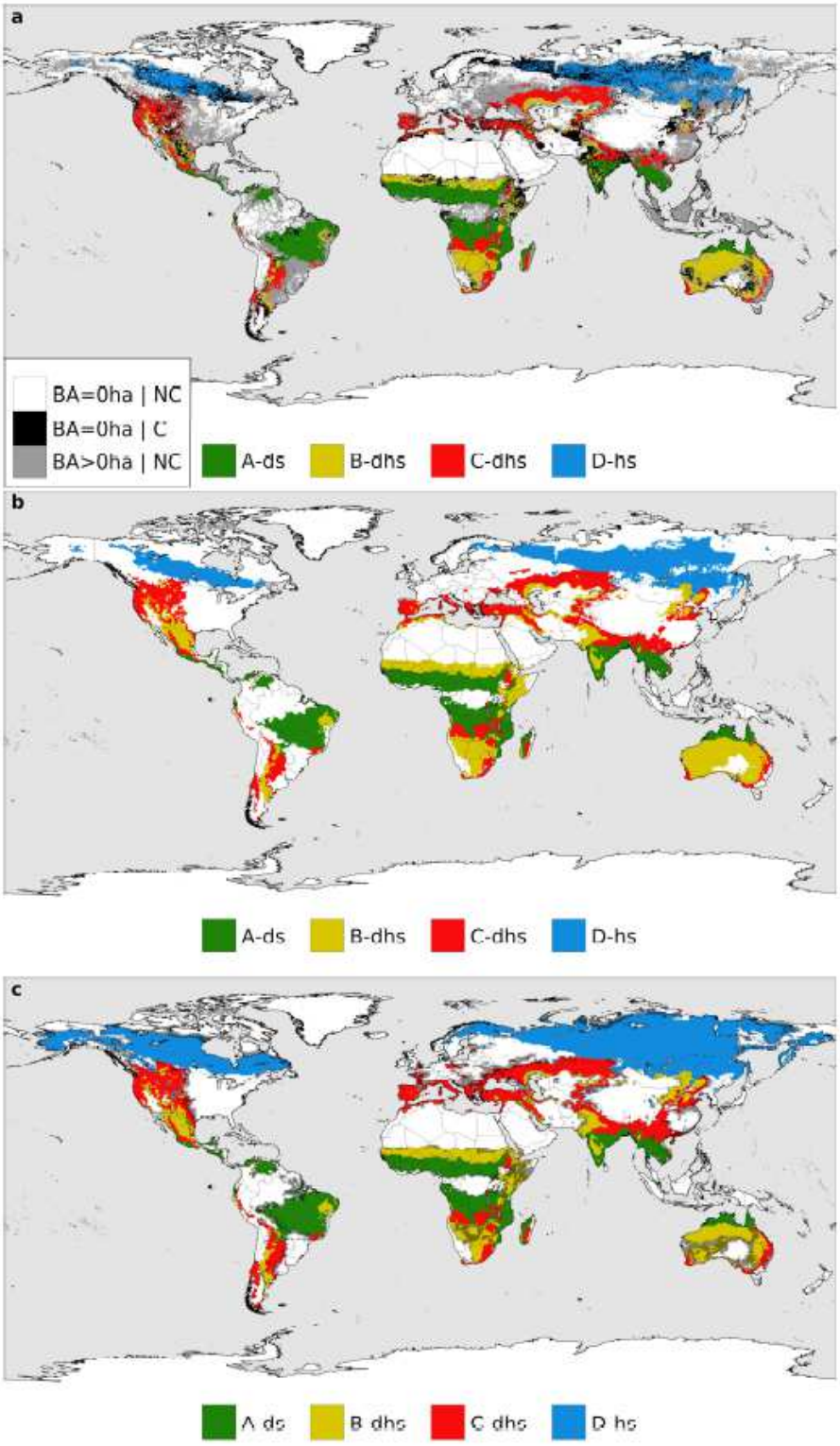

Figure 2

Fire-prone region classification. a, With observed burned area (BA) data as a reference: Not classified (NC, white) and misclassified (C, black) areas with BA=0ha, unclassified (NC, grey) and classified (A-ds, B-dhs, C-dhs and D-hs) areas with BA>0ha. b, Present (1996-2016) fire-prone climatic regions. c, Future (2070-2099) fire-prone climatic regions with shaded grey representing a <75% confidence percentage, estimated as the percentage of CMIP5 Global Circulation Models (GCMs) agreeing on the result. Note: The

designations employed and the presentation of the material on this map do not imply the expression of any opinion whatsoever on the part of Research Square concerning the legal status of any country, territory, city or area or of its authorities, or concerning the delimitation of its frontiers or boundaries. This map has been provided by the authors.

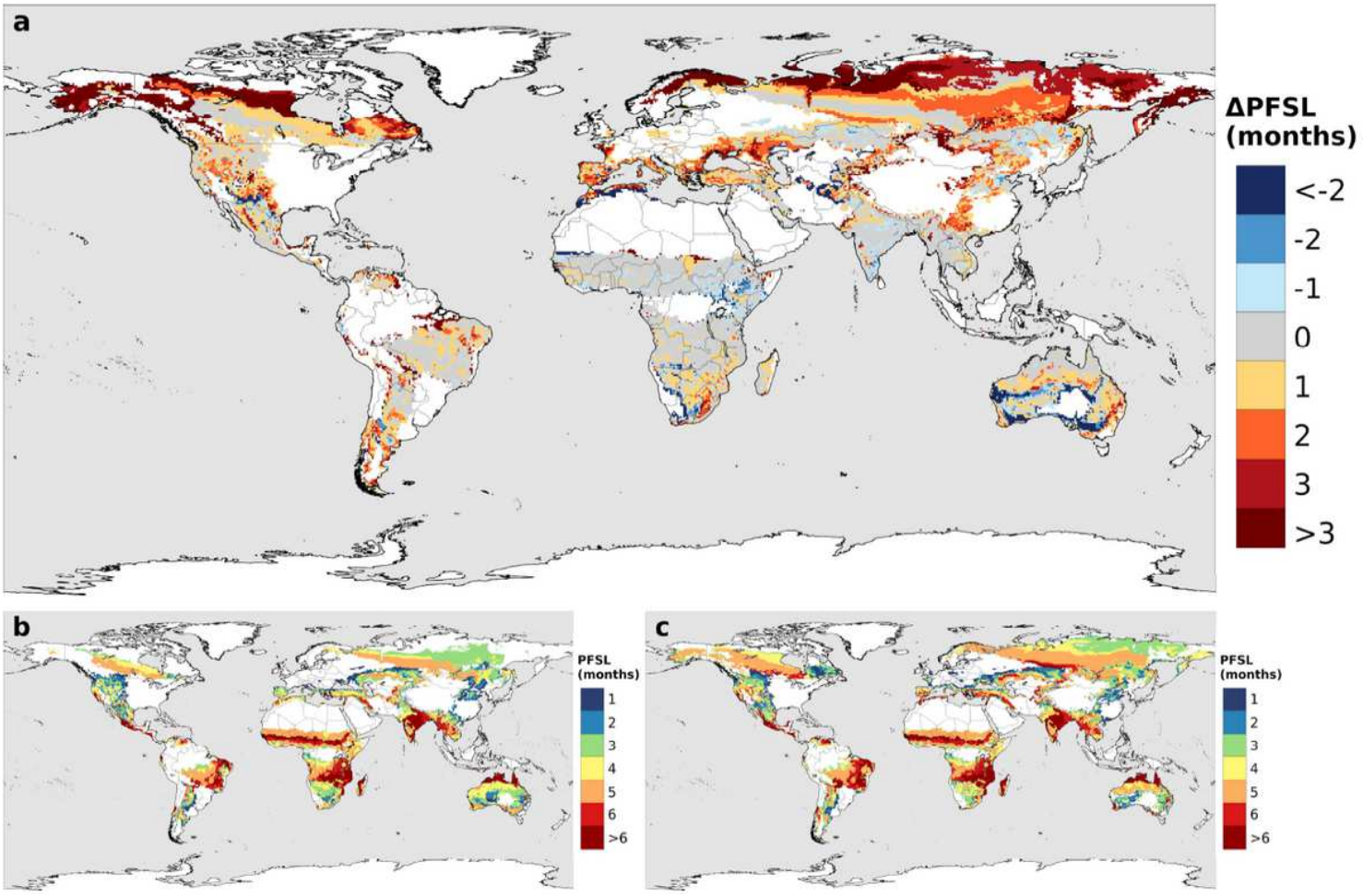

Figure 3

Potential Fire Season. a Future minus present Potential Fire Season Length (PFSL) difference in months (ΔPFSL). b, Present Potential Fire Season. c, Future Potential Fire Season. Note: The designations employed and the presentation of the material on this map do not imply the expression of any opinion whatsoever on the part of Research Square concerning the legal status of any country, territory, city or area or of its authorities, or concerning the delimitation of its frontiers or boundaries. This map has been provided by the authors.

Supplementary Files

This is a list of supplementary files associated with this preprint. Click to download.

- SupplementaryInformation.pdf